Automated Virtual Prototyping of Permanent Magnet Synchronous Machines for HEVs

Martin Hafner, Thomas Finken, Matthias Felden, and Kay Hameyer

Institute of Electrical Machines- RWTH Aachen University, Schinkelstraße 4, D-52062 Aachen, Germany

Ecological awareness has spurred a renewed interest in hybrid electrical vehicles (HEV), because of their ability to combine the drive power of a combustion engine with that of electrical machines. PMSM's notoriously offer large torque/weight ratios and are therefore particularly well suited for inclusion in HEV drivetrains, where the available space is in general strictly limited. The virtual prototyping and optimizing of PMSM for HEV drive trains is, however, a repetitive and computer intensive task. This paper presents a automated methodology aiming at reducing to a minimum the design time by means of a systematic approach and parallel computing.

***Index Terms*—AC-machines, design automation, design methodology, efficiency map, hybrid electrical vehicle, overall efficiency, permanent magnet synchronous machine (PMSM), software tools.**

I. Introduction

ELECTRIC and hybrid electric vehicles are the focus of an intense research activity nowadays. The contradictory requirements on the power train, such as high efficiency, high overload capacity and small installation space, make it so that many machine types are actually candidates for the electrified traction.

According to several comparative studies [1], [2], the permanent magnet synchronous machine (PMSM) appears to be best suited for such applications. In an earlier work by this author [3], a design and optimization procedure for an internal mounted PMSM (IPMSM) with fixed outer dimensions has been proposed, which determines the machines characteristics by different finite element (FE) simulations and corresponding post-processing routines. Since IPMSMs exhibit a strongly non-linear flux-current characteristic, all quantities such as induced voltage, synchronous and reluctance torque, optimal field weakening angle and inductances have to be computed explicitly at each considered operation point. This requires numerous 2D transient FE computations, leading to a high computational time and an additional time-consuming evaluation effort for the design engineer.

Therefore, all proposed routines and evaluation methods are combined into an automated tool chain that allows computing all machine characteristics of several design candidates. This method can be parallelized efficiently, so that, if enough computer resources are available, only four times the computation time of one FE simulation is necessary to run the whole design process. This allows considering more parameters in the design without increasing the development time proportionally.

II. Numerical Methods for an Automated Machine Computation

Since PMSMs exhibit (especially in case of rotors with buried magnets) a strongly nonlinear behavior, the design process has to consider saturation- and flux-leakage effects, which cannot be determined accurately by analytical formula, and quasi-static numerical FE simulations need to be performed for each geometry. Fig. 1 shows a flowchart describing an automated process for the calculation of all relevant machine characteristics. In the following, the function of each operational block in the chart is described. All simulations were conducted with the in-house FEM software package iMOOSE [4].

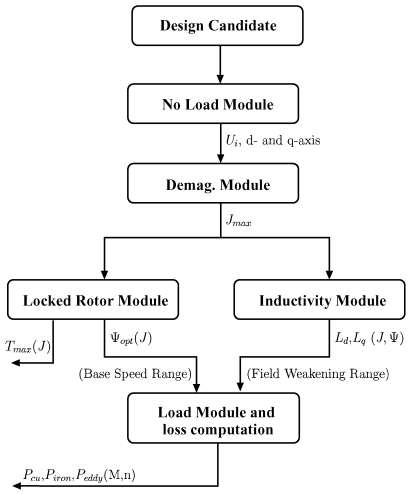

Fig. 1. Flowchart of the automated design process for a PMSM.

Initially, a ***No-Load Simulation*** is performed to calculate the stator phase flux-linkages and its time derivative, the back-emf, as well as to evaluate the occurring higher frequency harmonics. On basis of the motors maximal speed and DC link voltage U_{DC}, the designer can identify the best winding configuration. Moreover, this computation step detects the position of the d- and q-axis for further processing steps.

The electromagnetic overload capability of PM motors is limited by the demagnetization strength of the permanent magnet material. To determine the specific overload capability of a given design candidate, a ***Demagnetization Test*** is conducted. In worst case, e.g., by a fault in the power electronics and control, the maximum current is fed into the negative direct axis ($I_d = -I_{max}$) weakening the flux density inside the permanent magnets according to its demagnetization curve. The level of demagnetization should not lead to an irreversible demagnetization. In order to determine this physical limit, a current is fed into the negative direct axis whose magnitude is

Manuscript received May 28, 2010; accepted November 04, 2010. Date of current version April 22, 2011. Corresponding author: M. Hafner (e-mail: Martin.Hafner@IEM.RWTH-Aachen.de).

Color versions of one or more of the figures in this paper are available online at http://ieeexplore.ieee.org.

Digital Object Identifier 10.1109/TMAG.2010.2091675

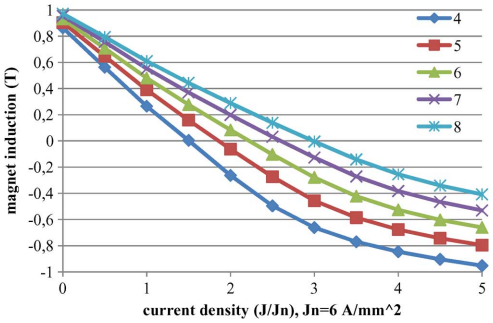

Fig. 2. Exemplary result of a demagnetization test for several magnet heights.

stepwise increased so as to determine the maximum current I_{max}, still having a working point on the linear part of the demagnetization characteristic. Fig. 2 shows the minimal flux density within the magnets as a function of the current density varying the thickness of the PM material.

The torque of an IPMSM $(X_q > X_d)$ is given by

$$T = \frac{3p}{\omega} \cdot [U_p - I_d \cdot (X_q - X_d)] \cdot I_q \tag{1}$$

where p is the pole pair number, ω the angular frequency and U_p the back-emf. It consists of the synchronous torque T_{syn} and the reluctance torque T_{rel}:

$$T = \underbrace{\frac{3p}{\omega} \cdot U_p I_q}_{T_{syn}} \underbrace{- \frac{3p}{\omega} \cdot I_q I_d \cdot (X_q - X_d)}_{T_{rel}}. \tag{2}$$

Inserting $I_q = I\cos\psi$, $I_d = I\sin\psi$, where ψ is the field-weakening angle, the torque can be rewritten as:

$$T = \hat{T}_{syn}\cos(\psi) - \hat{T}_{rel}\sin(2\psi) \tag{3}$$

i.e., the sum of a fundamental $(\hat{T}_{syn})$ and the first harmonic $(\hat{T}_{rel})$ which are constant for a given current. The phase voltage U_s is given by

$$U_s = U_p + \jmath X_q \underline{I}_q + \jmath X_d \underline{I}_d + R_1(\underline{I}_q + \underline{I}_d) \tag{4}$$

where R_1 is the phase resistance. For operation points in the base speed range (Region 1) the phase voltage U_s is below the maximum voltage, which in turn is limited by the dc-link voltage of the power converter, so that the phase current is constrained by the magnet demagnetization and further thermal limitations or the power electronic's maximal current. Differentiating (3) with respect to ψ, one sees that the maximum torque T_{max} per current (MTPA-control) is realized for the so called optimal field-weakening angle ψ_{opt}, cf. Fig. 3. The "***Locked-Rotor Test***" is thus made to determine the absolute values of the synchronous torque $\hat{T}_{syn}$ and the reluctance torque $\hat{T}_{rel}$, as well as to determine the optimal field-weakening angle ψ_{opt} and the maximum torque T_{max}. This calculation is performed for a stepwise increasing stator-current density in order to capture the dependency of those quantities on the load current as exemplified in Fig. 4.

For operation points in the field weakening range, the control strategy of the power converter limits the phase voltage to its maximum by shifting ψ. For the simulation of this control strategy (Region 2, in Fig. 3), the direct- and quadrature-axis inductances (L_d and L_q), which are both functions of the load current and the field weakening angle ψ, are calculated by means of the L_dL_q-***Computation***, see Fig. 5. By knowing the inductances L_d and L_q and a corresponding field weakening angle the electromagnetic torque for each operation point is given by (1). In some cases, according to the quantities L_d and L_q, there exists a operation point within the field weakening range, where a further increase of the rotor speed n requires the current to be reduced below its maximum. From here on (Region 3, in Fig. 3), the power controller follows the maximum torque per voltage curve (MTPV-control).

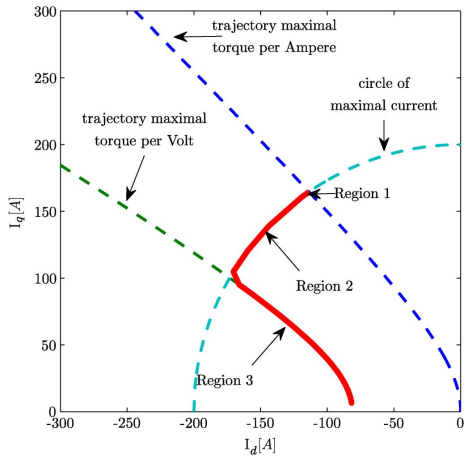

Fig. 3. PMSM operation points in the $I_d - I_q$ coordinate system.

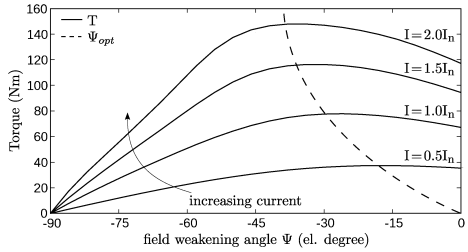

Fig. 4. The average torque over ψ, resulting from the "locked-rotor test".

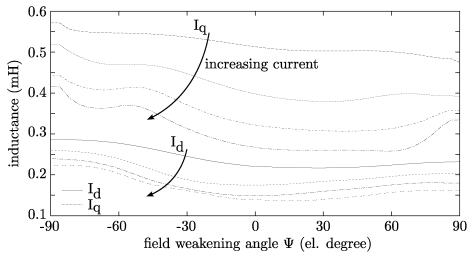

Fig. 5. Exemplary result of a inductance computation in function of the field weakening angle ψ and the current.

In order to evaluate and rate the motor's energy consumption and efficiency, all losses need to be determined for all operation points. This computation is conducted by the ***Operation Point Simulation***. At this step, the optimal field-weakening angle ψ_{opt} is used to set the maximum torque in the base speed range, whereas ψ has to be set by means of control strategies in the field weakening range. Ohmic losses P_{cu} are estimated taking end windings into account. Iron losses are computed by means of quasi-static numerical FE simulations and an improved post-processing formula based on the loss-separation principle [5], [6] considering rotational hysteresis losses as well. The imple-

mented formula assumes a separability of the iron losses (P_{Fe}) into hysteresis losses (P_h), eddy-current losses (P_{ec}) and excess losses (P_{ex})

$$P_{Fe} = P_h + P_{ec} + P_{ex} \tag{5}$$

where P_{ec} and P_{ex} are computed from the contributions of each harmonic of the flux density over one electrical period, whereas P_h is determined as a function of the peak value of the magnetic-flux density on the same time interval.

Eddy-current losses in permanent magnets (PM) are not covered by (5). Their evaluation is by nature a three-dimensional problem, but an estimation by 2D FEA leads to fair results in comparison to 3D transient FE-computations [7]. The deviation between both approaches depends on the geometry of the cross section, which requires for a precise prediction correction terms from 3D simulation. Since the computation of transient 3D-FE problems is, in comparison to 2D, rather time-consuming, this step is embedded in the process, but only executed for the group of final design candidates and therefore not mentioned as a separate standard block in the flowchart of Fig. 1. The computation time required for the whole procedure is discussed in Section IV. In this paper, the eddy-current density in PM's is calculated for each considered operation point by means of a transient 3D-FE approach, as described in [8], using the same time discretization as in 2D. The eddy-current density J_{ec} and the specific conductivity of the magnet material σ_{pm} are used to determine the eddy-current losses P_{magnet} by integration over the magnet's volume V_{pm}

$$P_{magnet} = \int \frac{1}{\sigma_{pm}} \vec{J}_{ec}^{2} dV_{pm}. \tag{6}$$

[9] shows, that the dependency of magnet losses on the number of axial segmentations n_{seg} can be written as

$$P_{magnet}(J, n_{seg}) = \lambda \left(\frac{n_{seg}}{n_{seg}^{max}} \right) P_{magnet}\left(J, n_{seg}^{max}\right) \tag{7}$$

where n_{seg}^{max} is a chosen maximal segmentation. 3D computations are done with nominal current to compute the correction factor λ for all considered axial segmentations, which will then be used for all other operation points.

By performing the loss calculation it is possible to determine the total losses P_{tot} for each operation point given by

$$P_{tot} = P_{cu} + P_{Fe} + P_{magnet} + P_{mech} \tag{8}$$

where P_{mech} are the mechanical losses depending on bearing and fan configurations-P_{mech} is neglected in this paper. In the machine's overall energy balance, the loss terms P_{Fe} and P_{magnet} are counteracting the electromagnetic torque T_{el}, because both energy terms are neglected in the electromagnetic FE governing equation, so that the measurable active torque can be expresses as

$$T_{act} = T_{el}(n, J, \psi) - \frac{P_{Fe}(n, J, \psi) + P_{magnet}(n, J, \psi)}{2\pi n}. \tag{9}$$

Resulting from the total losses and the input power P_{in},

$$P_{in} = 2\pi n \cdot T_{el}(n, J, \psi) + P_{cu}(J) \tag{10}$$

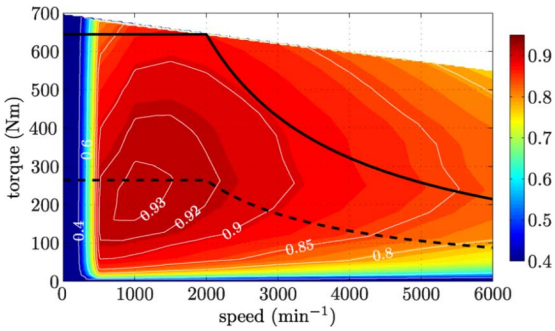

Fig. 6. Exemplary result of the efficiency of a PMSM according to (9)–(11).

the efficiency η can be calculated in function of speed and torque

$$\eta = \frac{2\pi n \cdot T_{act}(n, J, \psi)}{P_{in}(n, J, \psi)}. \tag{11}$$

Afterwards the results can be visualized as two-dimensional color maps, e.g. efficiency maps, as exemplary given in Fig. 6. In order to generate such a map, the Region 1 in Fig. 3 is discretized by N_{Map}^{1} operation points, whereas Region 2 and 3 are sampled by N_{Map}^{2} points. The best suited design candidates, are afterwards analyzed in detail over the whole operation range with respect to the motor efficiency. Therefore, the maps characterizing the machine's efficiency are fed into a vehicle-simulation model [10], which contains the vehicle data, the transmission, the battery, the battery controller and the main vehicle control unit.

III. The Aspect of Parallelization

The primary requirement of the development process for electrical machines (EM) in hybrid electrical vehicles (HEV) is to simulate each design candidate over its whole torque-speed characteristic. This is crucial, since an evaluation of the drive's mean lifetime or average efficiency is based on a driving cycle analysis, i.e. a stochastic distribution of operation points, [11]–[13]. The proposed design process, Fig. 1, is capable of this by computing the nonlinear machine characteristic, as well as the T-n diagram by numerous 2D transient, quasi-static FE computations. In consequence, the determination on the overall machine behavior requires a high computational effort. This leads, in the case of sequential processing, to a long simulation time. To limit and minimize this time delay in the design procedure, the necessary FE simulation, described in Section II, can be processed in parallel. Reorganizing the flowchart of Fig. 1 into a time-line diagram, given in Fig. 7, shows that the response time can be shorten to a minimal duration of four FE simulations. Since the computational blocks, such as ***No-Load Simulation*** and ***Demagnetization Test***, are interdependent, the load is unbalanced growing with each time-step (ΔT_{Fe}), where all modules to identify the machine characteristics are carried out by a current discretization of N_J. According to (1) a variation of the rotor speed n does not affect the quantities I_d, I_q and thus the variables J, ψ of the MTPA-control. Therefore, in case of base speed range, the discretization of the rotor speed (n-axis) in the efficiency maps can be replaced by rescaling (5) for a specific frequency f to an arbitrary frequency $\tilde{f}$ by

$$P_{Fe}(\tilde{f}) = P_h(f) \cdot c + P_{ec}(f) \cdot c^2 + P_{ex}(f) \cdot c^{1.5} \tag{12}$$

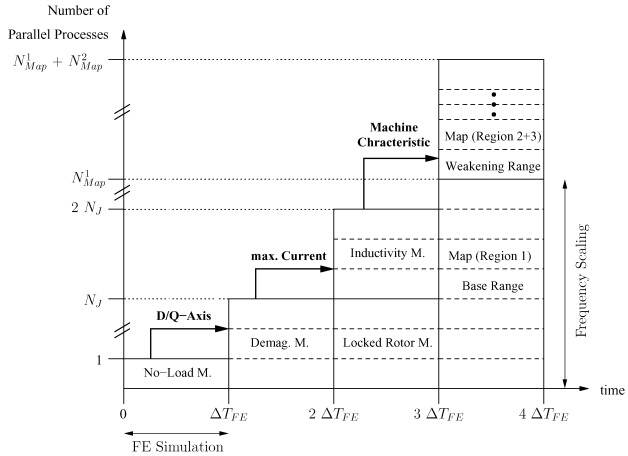

Fig. 7. Parallelization of the automated design process as line-line diagram, showing the necessary number of parallel processes in function of time.

where $c = \tilde{f}/f$. By this, the behavior in base speed range can be computed by N^1_{Map} current variations. Such a simplification is not applicable in Region 2 and 3 (MTPV-control), where the operation points need N^2_{Map} additional computations to be calculated explicitly. Therefore, N^2_{Map} is quite a bit larger than N^1_{Map}. The described automation process is integrated in the in-house software package ProMOTOR [14] which also manages the cluster computing.

IV. Discussion and Future Work

The automated virtual prototyping described in Section II and III has been applied in [3], [13] to design a 30 kW IPMSM for a total length limited to 160 mm and a volume limited to 9.2 dm^3. This project was part of the BMWi cooperative project Europa Hybrid [15] for a parallel hybrid electric vehicle. In the ongoing project phase, an adapted power converter has been designed and the prototype is presently under test. A comparison between simulation results and measurements will be presented in a future publication.

The quasi-static 2D-FE model has about 50,000 elements and requires, for a discretization of 90 steps per electric period, 15 minutes computation time (ΔT_{FE}). The load current is varied up to 3 times the nominal current in 13 steps (N_J, in Fig. 7). In the base speed range, the same current stepping is used (N^1_{Map}) and the flux weakening range requires 56 computations N^2_{Map}. The predesign step "***Locked-Rotor Test***" requires round about 30 minutes per design candidate (on a 15 node cluster) and a full evaluation of the efficiency map about 90 minutes.

The additional 3D computations with 200,000 elements last 7 hours with the same number of time steps, which shows why such an effort is spent for the best suited design candidates in a final stage only. Clearly, the accurate computation of magnet losses is a burden for the design and cannot be performed systematically, even with parallel computing. Appropriate modeling assumptions must be done to tackle this problem more efficiently, e.g., a 2D approach with an addition integrodifferential condition as proposed in [16].

V. Conclusion

In contrast to classical design approaches for PMSMs, requiring a specific torque and speed in one, sometimes in a few points, the main requirement for those drives in HEV applications is a high overall efficiency within a large range of the torque-speed characteristic, a high overload capacity and small installation space and weight.

This paper presents a formalism to design, evaluate and optimize the PMSM drive for its individual application purpose. The associated analysis is carried out as a flowchart based automated design process. To minimize overall simulation response time, the aspect of parallelization is considered as well. This allows considering a larger number of degrees-of-freedom, e.g. a wide design parameter space, to find the optimal parameter combination under given constraint for an individual application in short time. The proposed method already contributes in industrial projects and can be applied generally in the design of permanent magnet synchronous machine.

References

[1] M. Zeraoulia, M. Benbouzid, and D. Diallo, "Electric motor drive selection issues for HEV propulsion systems: A comparative study," *IEEE Trans. Veh. Technol.*, vol. 55, no. 6, pp. 1756–1764, 2006.

[2] T. Finken, M. Felden, and K. Hameyer, "Comparison and design of different electrical machine types regarding their applicability in hybrid electrical vehicles," in *Proc. 18th Int. Conf. on Electrical Machines*, 2008, pp. 1–5.

[3] T. Finken and K. Hameyer, "Design and optimization of an IPMSM with fixed outer dimensions for application in HEVs," in *Proc. IEEE Int. Conf. on Electric Machines and Drives*, 2009, pp. 1743–1748.

[4] D. van Riesen, C. Monzel, C. Kaehler, C. Schlensok, and G. Henneberger, "iMOOSE-an open-source environment for finite-element calculations," *IEEE Trans. Magn.*, vol. 40, no. 2, pp. 1390–1393, 2004.

[5] G. Bertotti, A. Boglietti, M. Chiampi, D. Chiarabaglio, F. Fiorillo, and M. Lazzari, "An improved estimation of iron losses in rotating electrical machines," *IEEE Trans. Magn.*, vol. 27, no. 6, pp. 5007–5009, 1991.

[6] M. H. Gracia, E. Lange, and K. Hameyer, "Numerical calculation of iron losses in electrical machines with a modified Post-Processing formula," presented at the 16th Int. Conf. Computation of Electromagnetic Fields, Aachen, Germany, 2007.

[7] S. Ruoho, T. Santa-Nokki, J. Kolehmainen, and A. Arkkio, "Modeling magnet length in 2-D finite-element analysis of electric machines," *IEEE Trans. Magn.*, vol. 45, no. 8, pp. 3114–3120, 2009.

[8] C. Kaehler and G. Henneberger, "Eddy-current computation in the claws of a synchronous claw-pole alternator in generator mode," *IEEE Trans. Magn.*, vol. 38, no. 2, pp. 1201–1204, Mar. 2002.

[9] T. Finken and K. Hameyer, "Computation of iron and eddy-current losses in IPM motors depending on the field weakening angle and current waveform," presented at the 14th Int. Symp. on Electromagnetic Fields, Arras, France, Sep. 2009.

[10] T. Markel, A. Brooker, T. Hendricks, V. Johnson, K. Kelly, B. Kramer, M. O'Keefe, S. Sprik, and K. Wipke, "ADVISOR: A systems analysis tool for advanced vehicle modeling," *J. Power Sources*, vol. 110, no. 2, pp. 255–266, 2002.

[11] D. Bucher, R. Nuscheler, W. Meyer, and H. Herzog, "Comparison of electrical machine types in hybrid drive trains: Induction machine vs. permanent magnet synchronous machine," in *Proc. 18th Int. Conf. on Electrical Machines*, 2008, pp. 1–6.

[12] H. Neudorfer, N. Wicker, and A. Binder, "Comparison of three different electric powertrains for the use in hybrid electric vehicles," in *Proc. 4th IET Conf. on Power Electronics, Machines and Drives*, 2008, pp. 510–514.

[13] T. Finken, M. Hafner, M. Felden, and K. Hameyer, "Design rules for energy efficient IPM motors in HEV applications," *Electromotion*, vol. 17, no. 3, pp. 143–154, Jul. 2010.

[14] M. Schöning and K. Hameyer, "Virtual product development for electrical motors," in *Proc. IEEE Int. Conf. on Electric Machines and Drives*, 2007, vol. 2, pp. 949–952.

[15] TÜV Rheinland, Verbundprojekt Europa-Hybrid innovativer PKW-Hybridantrieb für europa, 2006 [Online]. Available: http://www.hybrid-antriebe.org/web/projekte/vagabund.html

[16] A. Belahcen and A. Arkkio, "Permanent magnets models and losses in 2D FEM simulation of electrical machines," in *Proc. 19th Int. Conf. on Electrical Machines*, Rome, 2010, pp. 1–6.